Modeling power law absorption and dispersion in viscoelastic solids using a split-field and the fractional Laplacian[a)]

Bradley E. Treeby[b)] and B. T. Cox
Department of Medical Physics and Biomedical Engineering, University College London, Gower Street, London WC1E 6BT, United Kingdom

(Received 3 February 2014; revised 1 July 2014; accepted 16 August 2014)

The absorption of compressional and shear waves in many viscoelastic solids has been experimentally shown to follow a frequency power law. It is now well established that this type of loss behavior can be modeled using fractional derivatives. However, previous fractional constitutive equations for viscoelastic media are based on temporal fractional derivatives. These operators are non-local in time, which makes them difficult to compute in a memory efficient manner. Here, a fractional Kelvin-Voigt model is derived based on the fractional Laplacian. This is obtained by splitting the particle velocity into compressional and shear components using a dyadic wavenumber tensor. This allows the temporal fractional derivatives in the Kelvin-Voigt model to be replaced with spatial fractional derivatives using a lossless dispersion relation with the appropriate compressional or shear wave speed. The model is discretized using the Fourier collocation spectral method, which allows the fractional operators to be efficiently computed. The field splitting also allows the use of a *k*-space corrected finite difference scheme for time integration to minimize numerical dispersion. The absorption and dispersion behavior of the fractional Laplacian model is analyzed for both high and low loss materials. The accuracy and utility of the model is then demonstrated through several numerical experiments, including the transmission of focused ultrasound waves through the skull. © *2014 Acoustical Society of America*. [http://dx.doi.org/10.1121/1.4894790]

PACS number(s): 43.20.Bi, 43.20.Jr, 43.35.Cg [ANN] Pages: 1499–1510

I. INTRODUCTION

Accurately accounting for the absorption and dispersion of waves in lossy media is important in many branches of acoustics, including seismology,[1] geophysics,[2] ultrasonics,[3] photoacoustics,[4] and elastography.[5] Experimentally, the acoustic absorption in a wide range of materials relevant to these fields has been shown to follow a frequency power law of the form $\alpha_0\omega^y$, where α_0 is a proportionality coefficient, ω is the temporal frequency, and y is between 0 and 2.[6] It is now well established that this type of behavior can be modeled through the use of fractional derivative operators—a recent review is given by Holm and Näsholm.[7] However, previous constitutive equations that account for power law absorption in solid media are based on *temporal* fractional derivatives.[8] These operators are non-local in time, which means their numerical evaluation requires storing the time history of the field variables in memory. This can have a significant impact on the tractability of practical modeling problems. For example, Wismer used the time history of the wavefield for the previous 20 time steps to evaluate a power law absorption term based on the temporal fractional derivative,[9] Caputo used the previous 70 time steps,[10] while Norton and Novarini used the previous 1024 time steps.[11] The length of the time history required depends on the value of the power law exponent used, with values close to $y = 1$ the most computational demanding.[9] Unfortunately, this value corresponds to many materials of interest, for example, soft biological tissue in the MHz range where y is typically close to 1.[12] The memory required to evaluate the power law absorption term can thus be very significant, particularly in solid media where the field variables are represented by vectors and tensors.

To overcome the large memory requirements, several authors have discussed the construction of temporally local or *diffusive* schemes for the computation of temporal fractional derivatives.[13,14] This approach is based on expressing the fractional derivative in the frequency domain as an improper integral of a rational function, which is then approximated using a quadrature scheme.[15] In the time domain, each term in the quadrature sum corresponds to a convolution with an exponential kernel. This is equivalent to replacing the non-local problem with a series of local problems, which can be solved either as a system of first-order differential equations at each time step,[16,17] or recursively.[15] The accuracy of this approach depends strongly on the quadrature scheme and the number of integration points used to evaluate the integral.[15]

In the lossy acoustic case (where the medium is represented as a fluid rather than a viscoelastic solid), it is also possible to directly replace the fractional time derivatives with fractional space derivatives which are non-local in *space* rather than time.[18,19] If the Fourier collocation spectral method is used to discretize the spatial gradients,[20] these operators can be computed very efficiently without needing to access the time history of the field variables.[19] Here, we

[a)]Portions of this work were presented in "A computationally efficient elastic wave model for media with power-law absorption," IEEE International Ultrasonics Symposium, Prague, Czech Republic, 21–25 July 2013.
[b)]Author to whom correspondence should be addressed. Electronic mail: b.treeby@ucl.ac.uk

show how this idea can be extended to modeling the propagation of compressional and shear waves in viscoelastic solids with power law absorption. In Sec. II, the formulation of the model is described, including the fractional Kelvin-Voigt constitutive relation on which it is based. The absorption behavior of the fractional Laplacian wave equation is also analyzed. In Sec. III, the discretization and implementation of the model using the *k*-space pseudospectral method is discussed. Several numerical examples are then given to illustrate the capabilities of the developed model. Summary and discussion are presented in Sec. IV.

II. MODEL DEVELOPMENT

A. Kelvin-Voigt model

Before proceeding to a discussion of fractional constitutive equations, it will be beneficial to briefly revisit the formulation and behavior of the classical Kelvin-Voigt model. This discussion will form the basis for later analysis of more complex material behavior. In an elastic material, the stress and strain are related by the stiffness, which is a measure of the material's resistance to deformation in response to an applied force. For a general anisotropic medium, this relationship can be written using Einstein summation notation as

$$\sigma_{ij} = C_{ijkl}\varepsilon_{kl}, \tag{1}$$

where σ is the stress tensor, ε is the strain tensor, and C is the stiffness tensor. For small deformations, the strain and the particle displacement u are related by

$$\varepsilon_{ij} = \frac{1}{2}\left(\frac{\partial u_i}{\partial x_j} + \frac{\partial u_j}{\partial x_i}\right). \tag{2}$$

To account for viscoelastic behavior in which a time dependent strain creep is observed in response to an applied force, Eq. (1) is generalized by adding terms proportional to the temporal derivatives of the stress and strain,[8]

$$\left[1 + \sum_{m=1}^{M_1} A^m_{ijkl}\frac{\partial^m}{\partial t^m}\right]\sigma_{ij} = \left[C_{ijkl} + \sum_{m=1}^{M_2} B^m_{ijkl}\frac{\partial^m}{\partial t^m}\right]\varepsilon_{kl}. \tag{3}$$

This expression accounts for the four types of classical viscoelastic behavior (for example, the Maxwell or Zener models) depending on the values of A^m, B^m, M_1, M_2, and C.[8] When $M_1 = 0$ and $M_2 = 1$ (where the value of the empty sum is taken to be zero), the classical Kelvin-Voigt model is obtained,

$$\sigma_{ij} = C_{ijkl}\varepsilon_{kl} + N_{ijkl}\frac{\partial}{\partial t}\varepsilon_{kl}, \tag{4}$$

where N is the viscosity tensor. If the medium is isotropic, there are only two independent components of both the stiffness and viscosity tensors. The Kelvin-Voigt stress-strain relation can then be written in the form[21]

$$\sigma_{ij} = \lambda\delta_{ij}\varepsilon_{kk} + 2\mu\varepsilon_{ij} + \chi\delta_{ij}\frac{\partial}{\partial t}\varepsilon_{kk} + 2\eta\frac{\partial}{\partial t}\varepsilon_{ij}. \tag{5}$$

Here λ and μ are the Lamé parameters, where μ is the shear modulus (the ratio of shear stress and shear strain), and χ and η are the compressional and shear viscosity coefficients, respectively. The Lamé parameters are related to the shear and compressional sound speeds, c_s and c_p, by

$$\mu = \rho_0 c_s^2, \quad \lambda + 2\mu = \rho_0 c_\rho^2, \tag{6}$$

where ρ_0 is the ambient mass density.

To model the propagation of elastic waves, it is necessary to combine the appropriate stress-strain relation with Newton's second law. Written as a function of the stress and particle velocity, where $v_i = \partial u_i/\partial t$, this is given by

$$\frac{\partial v_i}{\partial t} = \frac{1}{\rho_0}\frac{\partial \sigma_{ij}}{\partial x_j}. \tag{7}$$

This expression is a statement of the conservation of momentum, sometimes referred to as the equation of motion. Using Eq. (2), the Kelvin-Voigt stress-strain relation can similarly be written as a function of the stress and particle velocity,

$$\frac{\partial \sigma_{ij}}{\partial t} = \lambda\delta_{ij}\frac{\partial v_k}{\partial x_k} + \mu\left(\frac{\partial v_i}{\partial x_j} + \frac{\partial v_j}{\partial x_i}\right) + \chi\delta_{ij}\frac{\partial^2 v_k}{\partial x_k \partial t} + n\left(\frac{\partial^2 v_i}{\partial x_j \partial t} + \frac{\partial^2 v_j}{\partial x_i \partial t}\right). \tag{8}$$

Equations (7) and (8) describe a set of coupled partial differential equations that account for the propagation of compressional and shear waves in an isotropic viscoelastic solid. These equations can also be combined into a single elastic wave equation. Written as a function of the particle displacement u, for a medium with homogeneous material properties this is given by[21]

$$\rho_0\frac{\partial^2 u_i}{\partial t^2} = (\lambda+\mu)\frac{\partial^2}{\partial x_i \partial x_j}u_j + \mu\frac{\partial^2}{\partial x_j^2}u_i + (\chi+\eta)\frac{\partial^2}{\partial x_i \partial x_j}\frac{\partial u_j}{\partial t} + \eta\frac{\partial^2}{\partial x_j^2}\frac{\partial u_i}{\partial t}. \tag{9}$$

Using vector notation, this is equivalent to

$$\rho_0\frac{\partial^2 \mathbf{u}}{\partial t^2} = (\lambda+\mu)\nabla(\nabla\cdot\mathbf{u}) + \mu\nabla^2\mathbf{u} + (\chi+\eta)\nabla\left(\nabla\cdot\frac{\partial \mathbf{u}}{\partial t}\right) + \eta\nabla^2\frac{\partial \mathbf{u}}{\partial t}. \tag{10}$$

Expanding the vector Laplacian using $\nabla^2\mathbf{u} = \nabla(\nabla\cdot\mathbf{u}) - \nabla\times(\nabla\times\mathbf{u})$ and replacing the Lamé parameters with the compressional and shear sound speeds from Eq. (6) then gives

$$\frac{\partial^2 \mathbf{u}}{\partial t^2} = c_p^2\nabla(\nabla\cdot\mathbf{u}) - c_s^2\nabla\times(\nabla\times\mathbf{u}) + \tau_p c_p^2\nabla\left(\nabla\cdot\frac{\partial \mathbf{u}}{\partial t}\right) - \tau_s c_s^2\nabla\times\left(\nabla\times\frac{\partial \mathbf{u}}{\partial t}\right), \tag{11}$$

where the parameters τ_p and τ_s are defined as

$$\tau_p = \frac{\chi + 2\eta}{\rho_0 c_p^2} = \frac{\chi + 2\eta}{\lambda + 2\mu}, \quad \tau_s = \frac{\eta}{\rho_0 c_s^2} = \frac{\eta}{\mu}. \tag{12}$$

To analyze the individual behavior of compressional and shear waves, Eq. (11) can also be written in terms of scalar and vector potentials, where $\mathbf{u} = \nabla\phi + \nabla \times \boldsymbol{\Psi}$ (this is sometimes called the Helmholtz decomposition),

$$0 = \nabla\left(\frac{\partial^2\phi}{\partial t^2} - c_p^2\nabla^2\phi - \tau_p c_p^2 \frac{\partial}{\partial t}\nabla^2\phi\right) + \nabla \times \left(\frac{\partial^2 \boldsymbol{\Psi}}{\partial t^2} - c_s^2\nabla^2\boldsymbol{\Psi} - \tau_s c_s^2 \frac{\partial}{\partial t}\nabla^2\boldsymbol{\Psi}\right). \tag{13}$$

Individual equations for the potentials can then be obtained by taking the divergence or curl of Eq. (13), where $\nabla \cdot \mathbf{u} = \nabla^2\phi$ and $\nabla \times \mathrm{u} = \nabla^2\boldsymbol{\Psi}$. This results in two separate wave equations given by equating the bracketed terms in Eq. (13) to 0. Each of these is in the form of Stokes' classical viscous wave equation.[22] The parameters τ_p and τ_s can thus be interpreted as relaxation times in the Stokes' sense. For $\omega\tau \ll 1$, Stokes' equation accounts for acoustic absorption that varies with the square of frequency while the sound speed is approximately constant (meaning there is no dispersion). For $\omega\tau \gg 1$, both the absorption and the sound speed vary with the square root of frequency.[22]

B. Fractional Kelvin-Voigt model

In the low frequency limit where $\omega\tau \ll 1$, the classical Kelvin-Voigt model described in Sec. II A accounts for acoustic absorption that is proportional to ω^2. However, as mentioned in Sec. I, the absorption experimentally observed in many materials of interest is proportional to ω^y, where y is between 0 and 2, and is often close to 1. To account for this behavior, the operator equation given in Eq. (3) can be generalized by replacing the integer time derivatives with fractional time derivatives,[8]

$$\left[1 + \sum_{m=1}^{M_1} A_{ijkl}^m \frac{\partial^{m+n-1}}{\partial t^{m+n-1}}\right]\sigma_{ij} = \left[C_{ijkl} + \sum_{m=1}^{M_2} B_{ijkl}^m \frac{\partial^{m+n-1}}{\partial t^{m+n-1}}\right]\varepsilon_{kl}, \tag{14}$$

where $n \in (0, 1]$ is a non-integer power. Again, depending on the values of M_1 and M_2, this expression accounts for fractional generalizations of the four types of classical viscoelastic behavior, including the fractional Maxwell, Kelvin-Voigt, and Zener models.[23,24] Physically, the introduction of the fractional derivative can be understood to change the shape of the strain creep and stress relaxation responses captured by the model.[8]

For $M_1 = 0$, $M_2 = 1$, and $n = y - 1$, Eq. (14) leads to the fractional Kelvin-Voigt model

$$\sigma_{ij} = C_{ijkl}\varepsilon_{kl} + N_{ijkl}\frac{\partial^{y-1}}{\partial t^{y-1}}\varepsilon_{kl}. \tag{15}$$

This particular stress-strain relation has been widely used to describe the behavior of viscoelastic materials in geomechanics.[25,26] In the isotropic case, the fractional Kelvin-Voigt model can be written in the form

$$\sigma_{ij} = \lambda\delta_{ij}\varepsilon_{kk} + 2\mu\varepsilon_{ij} + \chi\delta_{ij}\frac{\partial^{y-1}}{\partial t^{y-1}}\varepsilon_{kk} + 2\eta\frac{\partial^{y-1}}{\partial t^{y-1}}\varepsilon_{ij}. \tag{16}$$

Following the same steps used in Sec. II A to manipulate the classical Kelvin-Voigt model, this expression can also be written as a wave equation dependent on the scalar and vector potentials,

$$0 = \nabla\left(\frac{\partial^2\phi}{\partial t^2} - c_p^2\nabla^2\phi - \tau_p c_p^2 \frac{\partial^{y-1}}{\partial t^{y-1}}\nabla^2\phi\right) + \nabla \times \left(\frac{\partial^2 \boldsymbol{\Psi}}{\partial t^2} - c_s^2\nabla^2\boldsymbol{\Psi} - \tau_s c_s^2 \frac{\partial^{y-1}}{\partial t^{y-1}}\nabla^2\boldsymbol{\Psi}\right). \tag{17}$$

In this case, the equations for the individual potentials are now both in the form of the Caputo fractional wave equation.[9,26] Written in terms of the scalar potential ϕ, this is given by

$$\frac{1}{c_0^2}\frac{\partial^2}{\partial t^2}\phi - \nabla^2\phi - \tau\frac{\partial^{y-1}}{\partial t^{y-1}}\nabla^2\phi = 0. \tag{18}$$

In the low frequency limit where $\omega\tau \ll 1$, this equation encapsulates power-law acoustic absorption of the form[23,27]

$$\alpha \approx -\frac{\tau\cos(\pi y/2)}{2c_0}\omega^y, \tag{19}$$

where α is the absorption coefficient in $\mathrm{Np\,m^{-1}}$. Using the relaxation times defined in Eq. (12), when $\omega\tau_p \ll 1$ and $\omega\tau_s \ll 1$, the absorption of compressional and shear waves is thus governed by

$$\alpha_p \approx -\frac{(\chi + 2\eta)\cos(\pi y/2)}{2\rho_0 c_p^3}\omega^y, \quad \alpha_s \approx -\frac{\eta\cos(\pi y/2)}{2\rho_0 c_s^3}\omega^y. \tag{20}$$

Correspondingly, to account for absorption of the form $\alpha = \alpha_0\omega^y$ in the low frequency limit, the viscosity coefficients in the fractional Kelvin-Voigt model should be chosen such that

$$\eta = -\frac{2\rho_0 c_s^3}{\cos(\pi y/2)}\alpha_{0,s}, \quad \chi = -\frac{2\rho_0 c_p^3}{\cos(\pi y/2)}\alpha_{0,p} - 2\eta. \tag{21}$$

Here $\alpha_{0,s}$ and $\alpha_{0,p}$ are the desired absorption coefficient prefactors in $\mathrm{Np\,(rad/s)^{-y}\,m^{-1}}$ for shear and compressional waves, respectively, and y is the desired power law dependence.

C. From temporal to spatial fractional derivatives

As discussed in Sec. I, the use of fractional time derivatives in the stress-strain relation introduces a challenging computational problem. This arises because the temporal fractional operators are non-local in time, and thus their

numerical evaluation requires storing the time history of the field variables (unless a diffusive scheme is used). Under certain conditions, it is possible to replace fractional time derivatives with fractional space derivatives that are non-local in space, rather than time.[19] For explicit time-stepping methods, this has a significant computational benefit, as the wavefield at other spatial positions for each time step is already known.

To illustrate how this replacement arises, consider the Fourier transform of the fractional temporal derivative of a function $g(x, t)$,

$$\mathcal{F}_{x,t}\left\{\frac{\partial^y g(x,t)}{\partial t^y}\right\} = (-i\omega)^y G(k,\omega). \tag{22}$$

Here k and ω are the spatial and temporal frequencies, respectively, and $\mathcal{F}_{x,t}\{\cdots\}$ denotes the Fourier transform over x and t. The first part of this expression can be expanded using $(-i)^y = \cos(\pi y/2) - i\sin(\pi y/2)$ to give

$$(-i\omega)^y = \cos(\pi y/2)\omega^y + (-i\omega)\sin(\pi y/2)\omega^{y-1}. \tag{23}$$

For many applications, acoustic absorption only has a second order effect on wave propagation, i.e., $\omega\tau \ll 1$. This means that the temporal frequency terms in Eq. (23) (which correspond to temporal derivatives) can be replaced by spatial frequency terms (which correspond to spatial derivatives) using the dispersion relation for the lossless wave equation $\omega = c_0 k$. This is based on the premise that the substitution of first-order relations into second-order terms will result in third-order errors, which can be neglected.[28] Equation (23) then becomes

$$(-i\omega)^y \approx \cos(\pi y/2)k^y c_0^y + (-i\omega)\sin(\pi y/2)k^{y-1}c_0^{y-1}. \tag{24}$$

Using the definition of the fractional Laplacian[18]

$$\mathcal{F}_{x,t}\{(-\nabla^2)^y g(x,t)\} = k^{2y}G(k,\omega), \tag{25}$$

and taking the inverse Fourier transform of Eq. (24) then yields

$$\frac{\partial^y}{\partial t^y} \approx c_0^y \cos(\pi y/2)(-\nabla^2)^{y/2} + c_0^{y-1}\sin(\pi y/2)(-\nabla^2)^{(y-1)/2}\frac{\partial}{\partial t}. \tag{26}$$

Similarly for a fractional power of $y-1$,

$$\frac{\partial^{y-1}}{\partial t^{y-1}} \approx c_0^{y-1}\sin(\pi y/2)(-\nabla^2)^{(y-1)/2} - c_0^{y-2}\cos(\pi y/2)(-\nabla^2)^{(y-2)/2}\frac{\partial}{\partial t}. \tag{27}$$

Thus, fractional temporal derivatives can be replaced with fractional spatial derivatives without modifying the original absorption behavior, provided the effect of absorption on the wavefield is small.

To illustrate the utility of this relation, combining Eq. (27) with Eqs. (18)–(19) directly leads to the *fractional Laplacian wave equation*[7,18,19,29]

$$\frac{1}{c_0^2}\frac{\partial^2\phi}{\partial t^2} - \nabla^2\phi - \tau_1(-\nabla^2)^{y/2}\frac{\partial}{\partial t}\phi - \tau_2(-\nabla^2)^{(y+1)/2}\phi = 0. \tag{28}$$

Here the two proportionality coefficients are given by $\tau_1 = -2\alpha_0 c_0^{y-1}$ and $\tau_2 = 2\alpha_0 c_0^y \tan(\pi y/2)$. If the Fourier collocation spectral method is used to compute the spatial gradients, the fractional Laplacian terms become simple to compute, where

$$(-\nabla^2)^y g(x,t) = \mathcal{F}_x^{-1}\{k^{2y}\mathcal{F}_x\{g(x,t)\}\}. \tag{29}$$

This is the absorption model used in the open-source k-Wave toolbox for simulating the propagation of acoustic waves in fluid media with power law absorption.[30,31]

D. Absorption behavior of the fractional Laplacian wave equation

The fractional Laplacian wave equation given in Eq. (28) arises from a modification of the fractional term in the Caputo (or fractional Kelvin-Voigt) wave equation under the assumption that $\omega\tau \ll 1$. It is therefore of interest to investigate how the fractional Laplacian wave equation behaves when this condition is not met. This behavior can be extracted from the dispersion relation between k and ω, which is obtained by taking the Fourier transform of Eq. (28) over x and t (Ref. 29),

$$k^2 - \frac{\omega^2}{c_0^2} - 2i\alpha_0 c_0^{y-1}k^y\omega - 2\alpha_0 c_0^y\tan(\pi y/2)k^{y+1} = 0. \tag{30}$$

The conventional approach for studying the absorption and dispersion of equations in this form is to let $\omega \in \mathbb{R}$ and $k \in \mathbb{C}$, where $k = k_r + ik_i$. The absorption can then be extracted by solving for k_i.[22] However, for Eq. (30), the fractional powers of k prevent a solution from being easily obtained, except in the low frequency limit.[19] Alternatively, the absorption can be studied by letting $k \in \mathbb{R}$ and $\omega \in \mathbb{C}$, where $\omega = \omega_r - i\omega_i$.[32] This is motivated by considering the absorption of a traveling plane wave which can be specified using either a complex spatial frequency, or a complex temporal frequency, i.e.,

$$\begin{aligned} e^{i(kx-\omega t)} &= e^{i(k_r x-\omega t)}e^{-k_i x} \quad \text{where} \quad k = k_r + ik_i \\ e^{i(kx-\omega t)} &= e^{i(kx-\omega_r t)}e^{-\omega_i t} \quad \text{where} \quad \omega = \omega_r - i\omega_i. \end{aligned} \tag{31}$$

Considering the decay in amplitude of a plane wave after traveling a distance x in time t, the spatial and temporal absorption can be related by

$$\omega_i = \frac{x}{t}k_i = c_d k_i, \tag{32}$$

where c_d is the dispersive sound speed, i.e., the sound speed for a particular ω-k pair.

Returning to Eq. (30) and solving for ω using the quadratic formula leads to

$$\omega = -i\alpha_0 c_0^{y+1} k^y \pm c_0 k\sqrt{1-\zeta}, \tag{33}$$

where

$$\zeta = \alpha_0^2 c_0^{2y} k^{2y-2} + 2\alpha_0 c_0^y \tan(\pi y/2) k^{y-1}. \tag{34}$$

Interestingly, Eqs. (33) and (34) illustrate there is a threshold value of k where $\zeta > 1$ and thus the solution for ω becomes completely imaginary (this corresponds to the poles of the corresponding Green's function lying on the imaginary axis[29]). In this regime, the waves experience exponential decay without any temporal oscillations, analogous to evanescent waves.[33] Solving for the real and imaginary parts of $\omega \in \mathbb{C}$ in Eq. (33) then leads to

$$\begin{aligned} \omega_r &= \begin{cases} \pm c_0 k\sqrt{1-\zeta} & \text{if} \quad \zeta < 1 \\ 0 & \text{if} \quad \zeta > 1, \end{cases} \\ \omega_i &= \begin{cases} \alpha_0 c_0^{y+1} k^y & \text{if} \quad \zeta < 1 \\ \alpha_0 c_0^{y+1} k^y \mp c_0 k\sqrt{\zeta - 1} & \text{if} \quad \zeta > 1. \end{cases} \end{aligned} \tag{35}$$

When $\zeta < 1$, the fractional Laplacian wave equation exactly encapsulates power law absorption as a function of *spatial* frequency. The corresponding sound speed dispersion c_d is given by

$$c_d = \frac{\omega_r}{k} = \begin{cases} c_0\sqrt{1-\zeta} & \text{if} \quad \zeta < 1 \\ 0 & \text{if} \quad \zeta > 1. \end{cases} \tag{36}$$

This illustrates that the propagating part of the wave has a finite sound speed for all k.

The value of ζ along with the real and imaginary parts of ω and the dispersive sound speed c_d are plotted as a function of k in Fig. 1 using the ultrasonic properties of breast tissue in the MHz frequency range.[34] For these particular material properties, the value of k at the threshold $\zeta = 1$ is 5.6×10^9 rad/m. Using the first-order relationship $\omega = c_0 k$, this corresponds to a temporal frequency of 1.3 GHz. This is several orders of magnitude higher than the range of frequencies for which the absorption parameters are valid. A similar conclusion can be drawn using the absorption parameters and frequency range relevant to other applications. Consequently, the high wavenumber limit where $\omega_r = 0$ is unlikely to play a role in most practical modeling scenarios, particularly as any numerical solution will always be band-limited by the chosen discretization.

To calculate the corresponding absorption as a function of temporal frequency, which is how most experimental measurements are obtained, an explicit mapping can be made from ($\omega \in \mathbb{C}$, $k \in \mathbb{R}$) to ($\omega \in \mathbb{R}$, $k \in \mathbb{C}$) as defined in Eq. (31). Starting with the expression for ω_i when $\zeta < 1$ in Eq. (35) and substituting $\omega_i = c_d k_i$ from Eq. (32) into the left hand side and $k = \omega_r/c_d$ from Eq. (36) into the right hand side, and then replacing ω_r with ω leads to

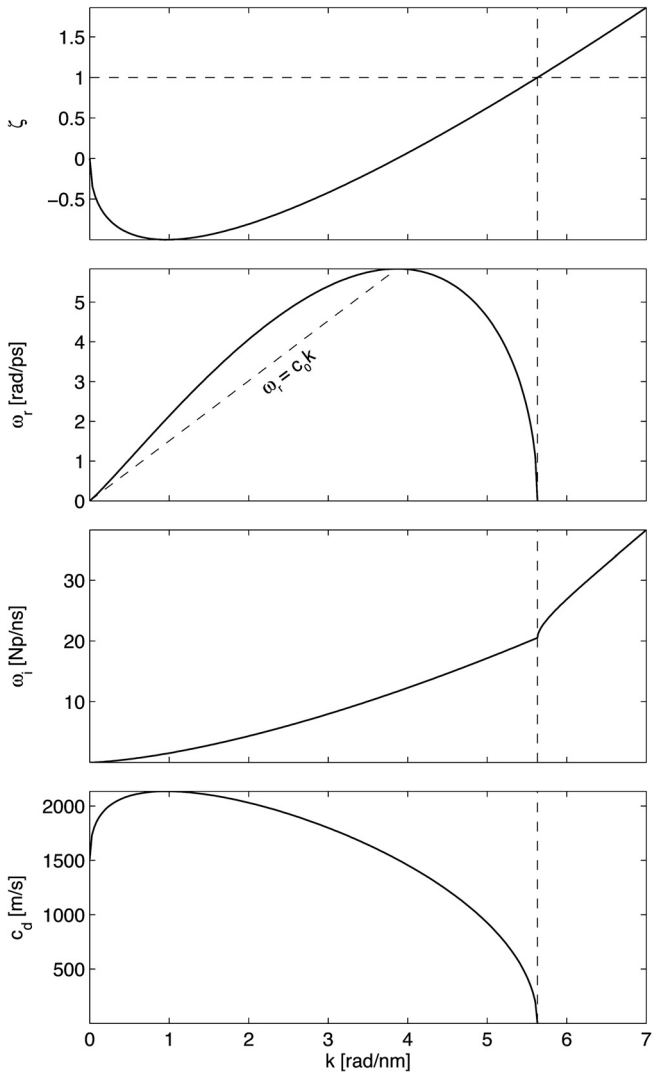

FIG. 1. Behavior of the fractional Laplacian wave equation as a function of k using the ultrasonic properties of compressional waves in breast tissue in the MHz range, where $\alpha_0 = 0.75$ dB/(MHz^y cm), $y = 1.5$, and $c_0 = 1510$ m/s (Ref. 34). For ω_r and ω_i, the positive square root is displayed. The vertical dashed lines indicate the threshold wavenumber where $\zeta = 1$. Above this threshold, ω_r and c_d are zero and the waves experience exponential decay without any temporal oscillations.

$$k_i = \frac{\alpha_0 c_0^{y+1} \omega^y}{c_d^{y+1}}. \tag{37}$$

Next, an expression for c_d as a function of ω can be obtained by substituting the first-order relation $\omega = c_0 k$ into Eq. (36) which gives

$$c_d \approx c_0\sqrt{1 - \alpha_0^2 c_0^2 \omega^{2y-2} - 2\alpha_0 c_0 \tan(\pi y/2)\omega^{y-1}}. \tag{38}$$

Combining these equations then yields the absorption behavior of the fractional Laplacian wave equation as a function of temporal frequency

$$k_i \approx \frac{\alpha_0 \omega^y}{\left(1 - \alpha_0^2 c_0^2 \omega^{2y-2} - 2\alpha_0 c_0 \tan(\pi y/2)\omega^{y-1}\right)^{(y+1)/2}}. \tag{39}$$

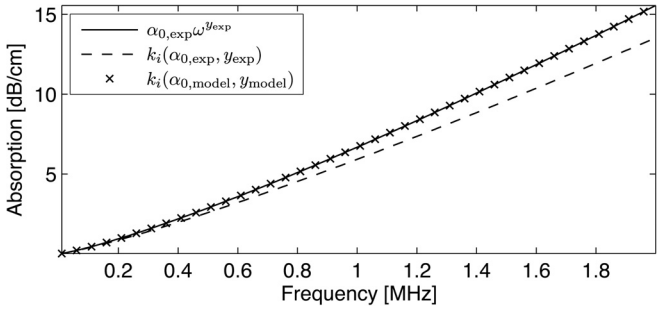

FIG. 2. Absorption behavior of the fractional Laplacian wave equation. For highly absorbing media, the encapsulated absorption (dashed line) will be smaller than a frequency power law calculated using the same pre-factor and exponent (solid line). However, using a simple fitting procedure, it is straightforward to select power law parameters that give the desired behavior (crosses).

When $\omega\tau \ll 1$, the absorption terms in the denominator are much less than 1, leaving $k_i \approx \alpha_0\omega^y$ as expected.[19] At intermediate values of $\omega\tau$ relevant to wave propagation in highly absorbing media,[23] the α_0^2 term can be neglected and the denominator can be expanded using the first two terms of a binomial series, leaving

$$k_i \approx \frac{\alpha_0\omega^y}{1-(y+1)\alpha_0 c_0 \tan(\pi y/2)\omega^{y-1}}. \tag{40}$$

Examining Eq. (40), when $1<y<2$, $\tan(\pi y/2)$ will be negative, meaning the denominator of Eq. (40) will be greater than one. Consequently, the power law absorption encapsulated by the fractional Laplacian wave equation for highly absorbing media will be smaller than that predicted by the low frequency asymptote of $\alpha_0\omega^y$. An example of this is given in Fig. 2 using the shear wave properties of skull bone in the MHz frequency range from Table I. The solid line illustrates the experimentally determined power law behavior $\alpha_{0,\mathrm{exp}}\omega^{y_{\mathrm{exp}}}$ (see discussion in Sec. III B), while the dashed line shows the absorption behavior of the fractional Laplacian wave equation calculated using Eq. (40) with the same power law parameters. To force the model to match the desired behavior over a specified frequency range, the appropriate power law absorption parameters $\alpha_{0,\mathrm{model}}$ and y_{model} to use in the fractional Laplacian wave equation can be obtained by solving a simple optimization problem, e.g.,

$$\underset{\alpha_{0,\mathrm{model}},y_{\mathrm{model}}}{\operatorname{argmin}} \; \| k_i(\alpha_{0,\mathrm{model}},y_{\mathrm{model}}) - \alpha_{0,\mathrm{exp}}\,\omega^{y_{\mathrm{exp}}} \|_2, \tag{41}$$

where k_i is the absorption behavior from Eq. (39) or (40). This minimization can be performed using any standard optimization tools, e.g., fminsearch in MATLAB. An example of this fitting procedure is given in Fig. 2, where the crosses illustrate the absorption behavior of the fractional Laplacian wave equation using the optimized parameters.

For completeness, the corresponding absorption behavior when $\omega\tau \gg 1$ and $\zeta > 1$ is given by

$$k_i \approx \sin(\pi/2y)\left(\frac{\omega}{2\alpha_0 c_0^{y+1}}\right)^{1/y}. \tag{42}$$

TABLE I. Material properties for skull bone based on the experimental data in White *et al.* (Ref. 40). Here ρ_0 is the mass density in kg/m^3, c_0 is the sound speed in m/s, α_0 is the power law absorption pre-factor in dB/(MHz^y cm), and y is the power law exponent. The values for $\alpha_{0,\mathrm{exp}}$ and y_{exp} were obtained by fitting a power law to the experimental data as shown in Fig. 5, while $\alpha_{0,\mathrm{model}}$ and y_{model} are the corresponding power law parameters that should be specified in the fractional Laplacian equation to observe this behavior numerically. Parameters marked with a * are the same for both compressional and shear waves.

	Compression	Shear
ρ_0	1732	*
c_0	2820	1500
$\alpha_{0,\mathrm{exp}}$	7.75	16.7
y_{exp}	1.37	*
$\alpha_{0,\mathrm{model}}$	8.83	19.5
y_{model}	1.43	*

When $y=2$, this reduces to $k_i \approx \frac{1}{2}\sqrt{\omega/(\alpha_0 c_0^3)}$ as expected for Stokes' equation when $\omega\tau \gg 1$.[22]

E. Field-splitting in *k*-space

As discussed in Sec. II D, the fractional Laplacian wave equation can be used to describe power law absorption over a wide range of frequencies and absorption values. However, in the elastic case, the compressional and shear waves travel at two different sound speeds. This means the lossless dispersion relation $\omega = c_0 k$ cannot be used with Eq. (23) to convert temporal fractional derivatives to spatial fractional derivatives. Here, an approach to overcome this restriction by splitting the particle velocity field into shear and compressional components is described.

Considering first the lossless case and following Ref. 35, the wave equation given in Eq. (11) can be written in the spatial frequency domain as

$$\frac{\partial^2 \mathbf{U}}{\partial t^2} = c_p^2 i\mathbf{k}\,(i\mathbf{k}\cdot\mathbf{U}) - c_s^2 i\mathbf{k}\times(i\mathbf{k}\times\mathbf{U}), \tag{43}$$

where $\mathcal{F}_x\{\nabla\} = i\mathbf{k}$ and $\mathcal{F}_x\{\mathbf{u}\} = \mathbf{U}$. The first term on the right hand side of this expression can be expanded using the substitution $\mathbf{k}(\mathbf{k}\cdot\mathbf{U}) = (\mathbf{k}\mathbf{k})\cdot\mathbf{U}$, where $\mathbf{k}\mathbf{k}$ is the dyadic tensor formed by the outer product of $\mathbf{k}$ with itself. Similarly, the second term can be expanded using the triple vector product $\mathbf{a}\times(\mathbf{b}\times\mathbf{c}) = \mathbf{b}\,(\mathbf{a}\cdot\mathbf{c}) - \mathbf{c}\,(\mathbf{a}\cdot\mathbf{b})$. This leads to $\mathbf{k}\times(\mathbf{k}\times\mathbf{U}) = (\mathbf{k}\mathbf{k} - k^2\mathbf{I})\cdot\mathbf{U}$, where $k^2 \equiv \mathbf{k}\cdot\mathbf{k}$ and $\mathbf{I}$ is the identity matrix. Using these expansions, Eq. (43) can then be written in the form

$$\frac{\partial^2 \mathbf{U}}{\partial t^2} = -k^2\left(c_p^2(\hat{\mathbf{k}}\hat{\mathbf{k}}) + c_s^2(\mathbf{I}-\hat{\mathbf{k}}\hat{\mathbf{k}})\right)\cdot\mathbf{U}, \tag{44}$$

where $\hat{\mathbf{k}} = \mathbf{k}/k$ is the normalized wavenumber vector.

The dyadic operators $(\hat{\mathbf{k}}\hat{\mathbf{k}})$ and $(\mathbf{I}-\hat{\mathbf{k}}\hat{\mathbf{k}})$ in Eq. (44) act to split the vector particle displacement into compressional and shear components, i.e.,

$$\mathbf{U}^p = (\hat{\mathbf{k}}\hat{\mathbf{k}})\cdot\mathbf{U}, \quad \mathbf{U}^s = (\mathbf{I}-\hat{\mathbf{k}}\hat{\mathbf{k}})\cdot\mathbf{U}, \tag{45}$$

where $\mathbf{U} = \mathbf{U}^p + \mathbf{U}^s$. Written using Einstein summation notation, this is equivalent to

$$U_i^p = \hat{k}_i \hat{k}_j U_j, \quad U_i^s = (\delta_{ij} - \hat{k}_i \hat{k}_j) U_j. \tag{46}$$

Using the same approach to split the particle velocity, the fractional Kelvin-Voigt stress-strain relation can be split into two equations which separately describe the compressional and shear components of the wavefield. Written in x-t space, this gives

$$\begin{aligned} \frac{\partial \sigma_{ij}^{p,s}}{\partial t} = {} & \lambda \left(\delta_{ij} \frac{\partial}{\partial x_k} v_k^{p,s} \right) + \mu \left(\frac{\partial}{\partial x_j} v_i^{p,s} + \frac{\partial}{\partial x_i} v_j^{p,s} \right) \\ & + \chi \left(\delta_{ij} \frac{\partial}{\partial x_k} \frac{\partial^{y-1}}{\partial t^{y-1}} v_k^{p,s} \right) \\ & + \eta \left(\frac{\partial}{\partial x_j} \frac{\partial^{y-1}}{\partial t^{y-1}} v_i^{p,s} + \frac{\partial}{\partial x_i} \frac{\partial^{y-1}}{\partial t^{y-1}} v_j^{p,s} \right), \end{aligned} \tag{47}$$

where the total stress field is $\sigma_{ij} = \sigma_{ij}^p + \sigma_{ij}^s$. Because the field is split, the fractional temporal derivatives can then be replaced with fractional spatial derivatives using Eq. (27), where c_0 is chosen to be the appropriate shear or compressional sound speed (this can be either homogeneous or heterogeneous).

Note, the definition of $n \in (0, 1]$ in Eq. (14) suggests that in the low frequency limit, the absorption power law dependence of the fractional Kelvin-Voigt model is restricted to $y \in (1, 2]$. However, in the case of the fractional Laplacian wave equation, there is no fundamental reason for this restriction, and the appropriate power law behavior can be observed both mathematically and numerically with $y \in (0, 2]$ and $y \neq 1$. Numerically, the split-field Kelvin-Voigt stress-strain relation also allows the possibility for the fractional power law exponent y to be defined separately for compressional and shear waves. However, this means the two wave types are no longer both governed by the constitutive equation given in Eq. (15), which only contains a single fractional operator. In most cases, choosing different power law exponents also causes the numerical model to become unstable. In light of this, the model discussed in Sec. III is restricted to a single value of y.

III. NUMERICAL MODEL

A. The *k*-space pseudospectral time domain solution

A computationally efficient model for elastic wave propagation in absorbing media can now be constructed using the split-field fractional Kelvin-Voigt model given in Eq. (47) along with the equation of motion given in Eq. (7). Here, these are solved as coupled partial differential equations using an explicit k-space pseudospectral method in which the Fourier collocation spectral method is used to compute spatial gradients,[20] and a k-space corrected finite difference scheme is used to integrate forward in time.[35–37] The discrete equations given below are written in compact notation, where the $+$ and $-$ symbols in the left superscript denote the field values at the next and current time steps, the p and s symbols denote the compressional and shear components of the field, the regular script i denotes the imaginary unit, terms including y in the right superscript indicate powers, and the i, j, l symbols in the right subscript denote Einstein summation indices, where a repeated index signifies a summation over all values of that index. The field variables are then updated in a time stepping fashion as follows:

(1) Update the Cartesian components of the particle velocity using both the compressional and shear parts of the stress tensor

$${}^{+}v_i = {}^{-}v_i + \frac{\Delta t}{\rho_0} \mathcal{F}^{-1} \left\{ i k_j \kappa^p \mathcal{F} \left\{ {}^{-}\sigma_{ij}^p \right\} + i k_j \kappa^s \mathcal{F} \left\{ {}^{-}\sigma_{ij}^s \right\} \right\}. \tag{48}$$

Here k_i represents the discrete set of wavenumbers in each Cartesian direction, k is the scalar wavenumber given by $k^2 = k_i k_i$, $\mathcal{F}\{\}$ is understood to be the spatial Fourier transform over all Cartesian dimensions, and κ is the k-space operator which corrects for the phase error introduced by the finite difference discretization of the time derivative, where $\kappa^{p,s} = \mathrm{sinc}(c_{\mathrm{ref}}^{p,s} k \Delta t/2)$ and $c_{\mathrm{ref}}^{p,s}$ is a reference sound speed chosen to be $c_{p,s}$ in a homogeneous medium (further discussion of the origin and behavior of the k-space operator can be found in Refs. 31, 35, 37, and 38).

(2) Split the Cartesian components of the particle velocity into compressional and shear parts using the k-space dyadic

$$\begin{aligned} V_i^p &= \hat{k}_i \hat{k}_j \mathcal{F}\{{}^{+}v_j\}, \\ V_i^s &= (\delta_{ij} - \hat{k}_i \hat{k}_j) \mathcal{F}\{{}^{+}v_j\}, \end{aligned} \tag{49}$$

where $\hat{k}_i = k_i / k$ is the normalized wavenumber.

(3) Calculate the fractional Laplacian power law absorption terms defined in Eq. (27)

$$\begin{aligned} L_i^{p,s} = {} & \mathcal{F}\{(c_{p,s}^{y-1} \sin(\pi y/2)) \mathcal{F}^{-1}\{k^{y-1} V_i^{p,s}\} \\ & - (c_{p,s}^{y-2} \cos(\pi y/2)) \mathcal{F}^{-1}\{k^{y-2} \partial_t V_i^{p,s}\}\}. \end{aligned} \tag{50}$$

Here, to avoid needing to explicitly calculate the temporal gradient of the particle velocity using a finite difference scheme, the $\partial_t V_i^{p,s}$ terms are calculated from the spatial gradients of the split stress field using the equation of motion from Eq. (7).

(4) Update the compressional and shear parts of the stress tensor using the corresponding components of the split velocity field

$$\begin{aligned} {}^{+}\sigma_{ij}^{p,s} = {} & {}^{-}\sigma_{ij}^{p,s} + \lambda \Delta t \mathcal{F}^{-1}\{\delta_{ij} i k_l \kappa^{p,s} V_l^{p,s}\} \\ & + \mu \Delta t \mathcal{F}^{-1}\{i k_j \kappa^{p,s} V_i^{p,s} + i k_i \kappa^{p,s} V_j^{p,s}\} \\ & + \chi \Delta t \mathcal{F}^{-1}\{\delta_{ij} i k_l L_l^{p,s}\} + \eta \Delta t \mathcal{F}^{-1}\{i k_j L_i^{p,s} + i k_i L_j^{p,s}\}, \end{aligned} \tag{51}$$

where the Lamé parameters and viscosity coefficients are calculated from the material properties using Eq. (6) and Eq. (21).

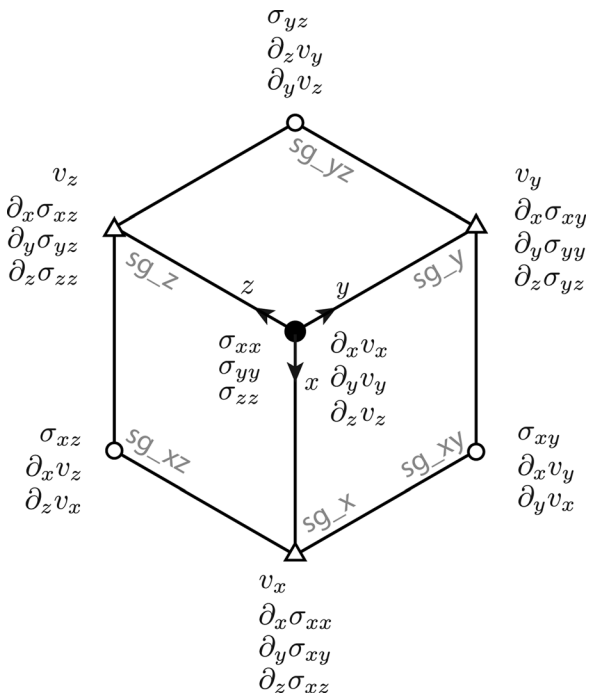

FIG. 3. Position of the field quantities and their derivatives on the staggered grid in three dimensions. The derivatives $\partial_i \partial_t v_j$ (etc.) are staggered the same way as the $\partial_i v_j$. terms.

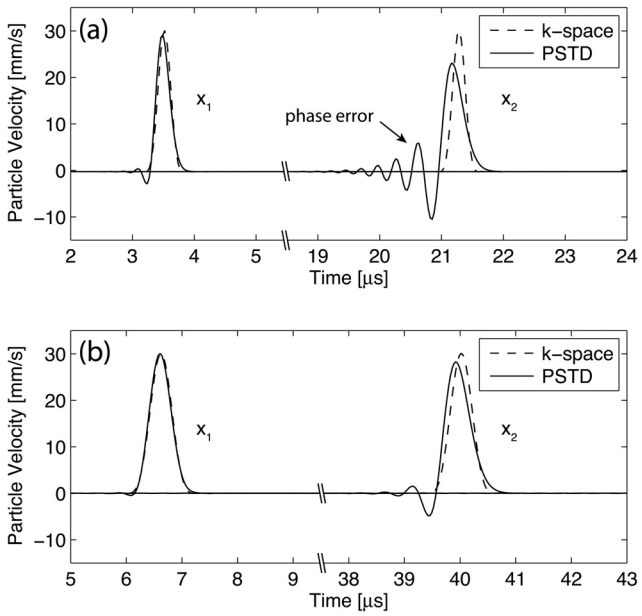

FIG. 4. Accumulation of phase error in the propagation of a unipolar plane wave pulse in a homogeneous medium with (dashed lines) and without (solid lines) the k-space correction term, where the latter is equivalent to a leapfrog pseudospectral time domain (PSTD) model. The two panels illustrate recorded time traces at positions $x_1 = 10$ mm and $x_2 = 60$ mm from the source for both (a) compressional and (b) shear waves.

To improve accuracy for simulations in heterogeneous media, a spatially staggered grid scheme is also used as shown in Fig. 3. In this case, translating the field quantities between the staggered grid points is achieved using the shift property of the Fourier transform.[35] The order of the update equations also means the stress and velocity quantities are temporally staggered. This is significant for the calculation of the $L_i^{p,s}$ terms in Eq. (50), as these require a combination of the staggered velocity and stress fields which are offset by $\Delta t/2$. The temporal grid staggering thus introduces a small phase error, which manifests as an error in the absorption and dispersion captured by the model. However, this error is typically small and can be controlled by modifying the size of the time step.[19]

In the general case of an absorbing and heterogeneous medium, it is difficult to derive a compact expression that describes the stability of the derived numerical model. However, the stability can also be determined numerically by re-writing Eqs. (48)–(51) into an update equation of the form ${}^{+}\mathbf{f} = \mathbf{A}^{-}\mathbf{f}$, where $\mathbf{f}$ is a vector containing the individual components of the particle velocity vector and stress tensor, and $\mathbf{A}$ is a update matrix that maps the values of the field variables from the current time step to the next. For a given set of material and grid parameters, the model will be stable if the absolute values of the eigenvalues of $\mathbf{A}$ do not exceed 1.[39] In general, the inclusion of the k-space correction term improves both the stability and the accuracy of the model.[35]

B. Numerical simulations

The model equations given in Sec. III A were implemented in MATLAB as an extension to the open-source k-Wave toolbox.[30] To demonstrate the ability of the model to accurately account for power law absorption and dispersion in solid media, several numerical experiments were performed using material properties relevant to biomedical ultrasound. First, to illustrate the effect of the k-space correction term on the accumulation of numerical phase error, a broadband unipolar plane wave pulse was propagated through a homogeneous and lossless medium. The grid size was set to be 32×512 grid points (9.375 mm $\times$ 150 mm) and the medium properties were set to be those of skull bone from Table I. The source was defined as a line-shaped initial particle velocity distribution with a magnitude of 0.1 m/s, which was smoothed using a frequency domain Blackman window to minimize the visual impact of the underlying band-limited interpolant.[29] This distribution was assigned to both v_x and v_y to simultaneously excite compressional and shear plane waves in the medium.

Figure 4 illustrates the particle velocity traces recorded 10 mm and 60 mm from the source, respectively, using a Courant-Friedrichs-Lewy (CFL) number of 0.3, where $\Delta t = \mathrm{CFL}\Delta x/c_{\max}$. The upper panel shows the compressional wave and the lower panel the shear wave, where the split components of the wavefield were extracted using Eq. (49). The dashed lines illustrate the recorded signals when the k-space correction is used, and the solid lines when κ in Eqs. (48) and (51) is set to 1, corresponding to a leapfrog pseudospectral time domain (PSTD) model. For a homogeneous medium, the inclusion of the k-space operator completely eliminates the phase error. In contrast, when the PSTD model is used, the accumulation of phase error is significant, even over the small domain size used in this example. This error can be controlled by reducing the size of the time step, or using a higher order scheme for the time integration. In the lossless case, as well as eliminating phase errors, the

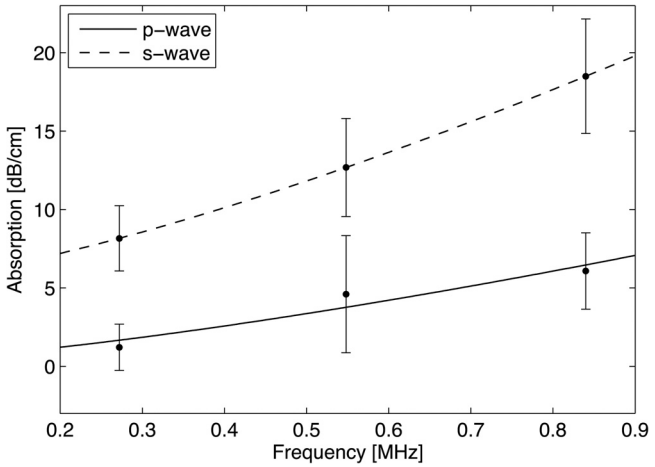

FIG. 5. Experimental data for the attenuation of ultrasound in skull bone from White *et al*. (Ref. 40) along with power law fits to the data.

inclusion of the *k*-space correction makes the model unconditionally stable.[35,37] Further discussion on the effect of the *k*-space operator for heterogeneous media is given in Ref. 31.

Next, to study the accuracy of the absorption and dispersion behavior captured by the numerical model, the same simulation was repeated for a lossy medium. The power law absorption parameters for skull bone were derived from the experimental data given by White *et al*.[40] The fits were obtained by simultaneously minimizing the L2 error between the power law expressions $\alpha_{0,p}\omega^y$ and $\alpha_{0,s}\omega^y$ and the experimental data. The data and fits are shown in Fig. 5, and the derived parameters are given in Table I. To obtain the corresponding power law parameters to use in the numerical model ($\alpha_{0,\text{model}}$ and y_{model} in Table I), the fitting procedure described in Sec. II D and Eq. (41) was used.

Figure 6 illustrates the absorption and dispersion behavior captured by the model. The model values were numerically extracted from the time traces recorded at 5 mm and 10 mm from the source using the expressions given in Eq. (34) in Ref. 19. The recorded traces for the compressional and shear wave are shown in Fig. 6(a), with the corresponding absorption and dispersion shown in Fig. 6(b) and Fig. 6(c). The open circles illustrate the absorption and dispersion behavior extracted from the model, while the solid lines illustrate the analytical values for comparison. There is a very close agreement, illustrating that the desired power law behavior is correctly captured by the model.

A final numerical example is shown in Fig. 7 to demonstrate the utility of the model for studying problems of practical interest. This example simulates the transmission of ultrasound from a focused transducer through the human skull. A similar setup was recently used experimentally by Legon *et al*.,[41] to demonstrate the feasibility of using transcranial focused ultrasound to non-invasively stimulate neural cells in the brain. The simulation was performed using a grid size of 576×768 grid points, a grid point spacing of 167 μm, a time step of 11.25 ns, and a total simulation time of 45 μs. The properties for the background medium were set to lossless water, where $c_p = 1481\ \text{ms}^{-1}$, $c_s = 0\ \text{ms}^{-1}$, and

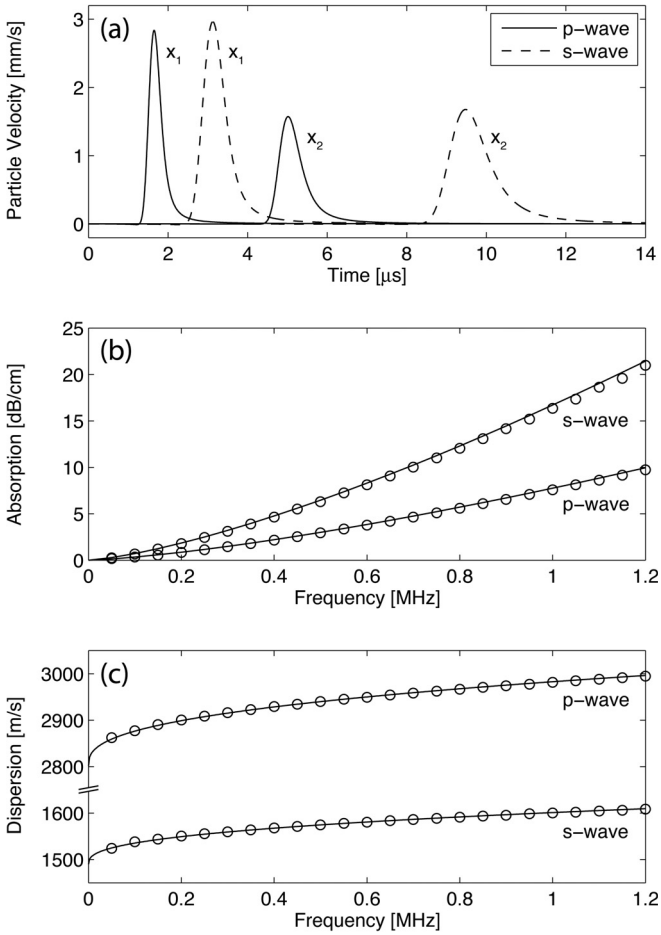

FIG. 6. Power law absorption and dispersion of compressional and shear waves in a viscoelastic solid given by the properties of bone. (a) Shape of the compressional and shear waves recorded at positions $x_1 = 5$ mm and $x_2 = 10$ mm from the source. (b) Absorption behavior captured by the model (open circles) compared with the analytical values (solid line). (c) Dispersion behavior captured by the model (open circles) compared with the analytical values (solid line).

$\rho_0 = 998\ \text{kg m}^{-3}$, while the layer of skull bone was assigned the properties given in Table I. The skull was defined as a circular disk with an outer radius of 8.75 cm and a thickness of 6.5 mm, and was smoothed using a frequency domain Blackman window.[30] The source was defined as a 30 mm line source with a 30 mm focal length (defined using electronic delays). The source signal was a three cycle tone burst centered at 0.5 MHz and was injected as a velocity source in the *y*-direction.

Three snapshots of the evolution of the wavefield are shown in Fig. 7(a)–7(c), with the position of the skull layer outlined with the dashed lines. The temporal maximum of the particle velocity magnitude recorded at each grid point during the simulation is shown in Fig. 7(d). For comparison, the equivalent result calculated using a lossless elastic wave model is shown in Fig. 7(e). When absorption is included, the magnitude of the particle velocity in the focus (shown with the black crosses) is reduced by 30%. This is particularly important in the context of neurostimulation, as the amplitude of the ultrasound waves is closely related to the observed neurological response.[42] Studying the magnitude and distribution of ultrasound within the skull under

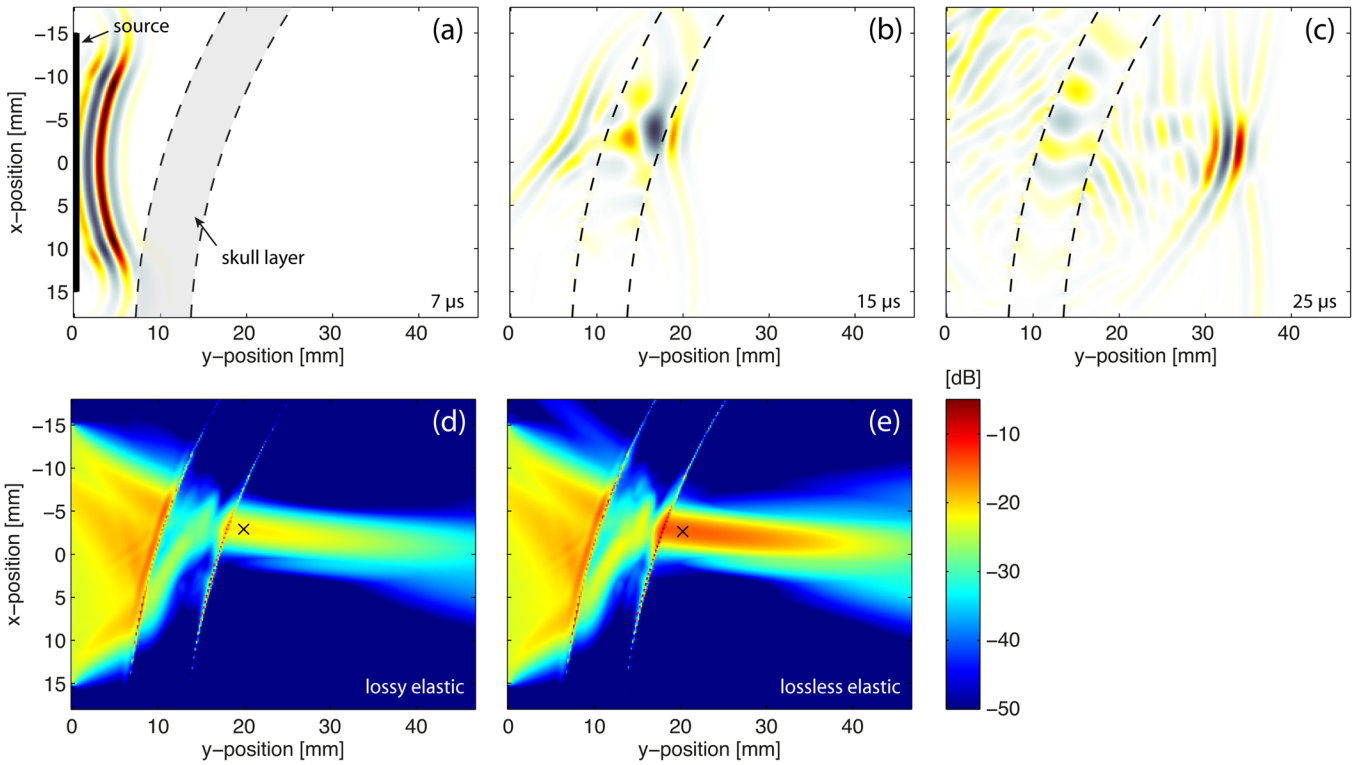

FIG. 7. (Color online) Simulation of the transmission of ultrasound waves generated by a focused transducer through a layer of skull bone. The upper three panels show snapshots of the normal stress after (a) 7 μs, (b) 15 μs, and (c) 25 μs. The position of the skull layer is denoted using the dashed lines. The lower two panels illustrate the temporal maximum value of the particle velocity magnitude recorded at each grid point over the duration of the simulation both (d) with, and (e) without absorption. The black crosses indicate the position of the focus inside the skull. When absorption is included, the magnitude at the focus is reduced by 30%.

different sonication conditions is one potential future application of the model.

Regarding computational efficiency, using double precision arithmetic, the total compute time for the lossy elastic simulation was 39 min 49 s, while the corresponding compute time for the lossless elastic simulation was 16 min 17 s. The difference for the lossless case is almost entirely due to the reduction in the number of forward and inverse FFTs required per time step. In two-dimensions, the lossy elastic model uses 70 2D-FFTs per time step, while the lossless model uses only 28. The additional FFTs are required to compute the absorption terms given in Eq. (50). In comparison, using a lossy fluid model (kspaceFirstOrder2D from the k-Wave toolbox), the compute time for an equivalent simulation was 7 min 45 s, where only 11 2D-FFTs are needed per time step. Note, in terms of the absolute compute times, using C++ instead of MATLAB and performing computations in single precision can increase the performance of the k-space model by a factor of $\sim$15.[43]

Compared to a non-split implementation, the use of the field-splitting approach approximately doubles the amount of memory and the number of compute operations needed per time step. However, this is a relatively small penalty compared to models based on temporal fractional derivatives which require storing the time history of the particle velocity at each grid point, in addition to evaluating a time convolution for each time step. The use of field-splitting also allows the inclusion of the k-space correction term. This minimizes the phase error introduced by the finite difference discretization of the temporal gradients, which in turn allows larger time steps to be used for the same degree of accuracy.[35]

IV. SUMMARY

A computationally efficient model that accounts for power law absorption and dispersion in viscoelastic solids is derived. This is based on a fractional Kelvin-Voigt constitutive equation which is split into compressional and shear wave components using a dyadic wavenumber tensor. The field-splitting allows the temporal fractional derivatives in the Kelvin-Voigt model to be replaced with spatial fractional derivatives using the lossless dispersion relation $\omega = c_0 k$, where c_0 is the appropriate compressional or shear wave speed. This replacement is significant, as the absorption term can then be efficiently evaluated using standard numerical techniques, without the need to store the time history of the wavefield. Here, the derived governing equations are discretized using the k-space pseudospectral method which allows the fractional operators to be easily computed in the spatial frequency domain. The field splitting approach also allows a k-space corrected finite difference scheme to be used for time integration, which minimizes the accumulation of phase errors.

The fractional Laplacian wave equation is shown to exhibit two distinct modes of behavior depending on the value of the spatial wavenumber relative to a high-wavenumber threshold. Above the threshold, the waves no longer

propagate and are subject to exponential decay without any temporal oscillations. However, in practice, the very high value of the threshold means this behavior is unlikely to contribute to most modeling scenarios. Below the threshold, the model exactly accounts for power law absorption as a function of spatial frequency. When $\omega\tau \ll 1$, this equates to power law absorption as a function of temporal frequency as expected. At intermediate values of $\omega\tau$, the absorption as a function of temporal frequency is smaller than the corresponding power law. However, using a simple fitting procedure, it is straightforward to select model parameters to give the desired behavior. Consequently, the fractional Laplacian Kelvin-Voigt model can be used to model wave propagation in a wide variety of materials with both low and high absorption values.

ACKNOWLEDGMENTS

This work was supported by the Dosimetry for Ultrasound Therapy project which is part of the European Metrology Research Programme (EMRP). The EMRP is jointly funded by the EMRP participating countries within EURAMET and the European Union. The authors would like to thank Jiri Jaros for discussion on the efficient implementation of Fourier spectral methods, and Bob Schoonover for discussion on power law absorption in elastic media.

[1]B. Ursin and T. Toverud, "Comparison of seismic dispersion and attenuation models," Stud. Geophys. Geod. **46**, 293–320 (2002).
[2]M. J. Buckingham, "Theory of acoustic attenuation, dispersion, and pulse propagation in unconsolidated granular materials including marine sediments," J. Acoust. Soc. Am. **102**, 2579–2596 (1997).
[3]T. L. Szabo, "Time domain wave equations for lossy media obeying a frequency power law," J. Acoust. Soc. Am. **96**, 491–500 (1994).
[4]B. E. Treeby, "Acoustic attenuation compensation in photoacoustic tomography using time-variant filtering," J. Biomed. Opt. **18**, 036008 (2013).
[5]K. H. Lee, B. A. Szajewski, Z. Hah, K. J. Parker, and A. M. Maniatty, "Modeling shear waves through a viscoelastic medium induced by acoustic radiation force," Int. J. Numer. Meth. Biomed. Eng. **28**, 678–696 (2012).
[6]T. L. Szabo and J. Wu, "A model for longitudinal and shear wave propagation in viscoelastic media," J. Acoust. Soc. Am. **107**, 2437–2446 (2000).
[7]S. Holm and S. P. Näsholm, "Comparison of fractional wave equations for power law attenuation in ultrasound and elastography," Ultrasound Med. Biol. **40**, 695–703 (2014).
[8]F. Mainardi, *Fractional Calculus and Waves in Linear Viscoelasticity* (Imperial College Press, London, 2010), pp. 23–76.
[9]M. G. Wismer, "Finite element analysis of broadband acoustic pulses through inhomogenous media with power law attenuation," J. Acoust. Soc. Am. **120**, 3493–3502 (2006).
[10]M. Caputo, J. M. Carcione, and F. Cavallini, "Wave simulation in biologic media based on the Kelvin-voigt fractional-derivative stress-strain relation," Ultrasound Med. Biol. **37**, 996–1004 (2011).
[11]G. V. Norton and J. C. Novarini, "Including dispersion and attenuation in time domain modeling of pulse propagation in spatially-varying media," J. Comput. Acoust. **12**, 501–519 (2004).
[12]F. A. Duck, *Physical Properties of Tissue: A Comprehensive Reference Book* (Academic Press, San Diego, CA, 1990), pp. 73–135.
[13]L. Yuan and O. P. Agrawal, "A numerical scheme for dynamic systems containing fractional derivatives," J. Vib. Acoust.-Trans. ASME **124**, 321–324 (2002).
[14]K. Diethelm, "An investigation of some nonclassical methods for the numerical approximation of Caputo-type fractional derivatives," Numer. Algorithms **47**, 361–390 (2008).
[15]C. Birk and C. Song, "An improved non-classical method for the solution of fractional differential equations," Comput. Mech. **46**, 721–734 (2010).
[16]J.-F. Deü and D. Matignon, "Simulation of fractionally damped mechanical systems by means of a Newmark-diffusive scheme," Comput. Math. Appl. **59**, 1745–1753 (2010).
[17]E. Blanc, G. Chiavassa, and B. Lombard, "Biot-JKD model: Simulation of 1D transient poroelastic waves with fractional derivatives," J. Comput. Phys. **237**, 1–20 (2013).
[18]W. Chen and S. Holm, "Fractional Laplacian time-space models for linear and nonlinear lossy media exhibiting arbitrary frequency power-law dependency," J. Acoust. Soc. Am. **115**, 1424–1430 (2004).
[19]B. E. Treeby and B. T. Cox, "Modeling power law absorption and dispersion for acoustic propagation using the fractional Laplacian," J. Acoust. Soc. Am. **127**, 2741–2748 (2010).
[20]J. P. Boyd, *Chebyshev and Fourier Spectral Methods* (Dover Publications, Mineola, NY, 2001), pp. 1–93.
[21]H. F. Pollard, *Sound Waves in Solids* (Pion Limited, London, 1977), pp. 203–233.
[22]J. J. Markham, R. T. Beyer, and R. B. Lindsay, "Absorption of sound in fluids," Rev. Mod. Phys. **23**, 353–411 (1951).
[23]S. Holm and R. Sinkus, "A unifying fractional wave equation for compressional and shear waves," J. Acoust. Soc. Am. **127**, 542–559 (2010).
[24]S. Holm and S. P. Nasholm, "A causal and fractional all-frequency wave equation for lossy media," J. Acoust. Soc. Am. **130**, 2195–2202 (2011).
[25]L. Knopoff, "On the dissipative viscoelastic constants of higher order," J. Acoust. Soc. Am. **26**, 183–186 (1954).
[26]M. Caputo, "Linear models of dissipation whose Q is almost frequency independent-II," Geophys. J. R. Astron. Soc. **13**, 529–539 (1967).
[27]J. F. Kelly and R. J. McGough, "Fractal ladder models and power law wave equations," J. Acoust. Soc. Am. **126**, 2072–2081 (2009).
[28]M. J. Lighthill, "Viscosity effects in sound waves of finite amplitudes," in *Surveys in Mechanics*, edited by G. K. Batchelor and R. M. Davies (Cambridge University Press, Cambridge, UK, 1956), pp. 250–351.
[29]B. E. Treeby and B. T. Cox, "A k-space Greens function solution for acoustic initial value problems in homogeneous media with power law absorption," J. Acoust. Soc. Am. **129**, 3652–3660 (2011).
[30]B. E. Treeby and B. T. Cox, "k-Wave: MATLAB toolbox for the simulation and reconstruction of photoacoustic wave fields," J. Biomed. Opt. **15**, 021314 (2010).
[31]B. E. Treeby, J. Jaros, A. P. Rendell, and B. T. Cox, "Modeling nonlinear ultrasound propagation in heterogeneous media with power law absorption using a k-space pseudospectral method," J. Acoust. Soc. Am. **131**, 4324–4336 (2012).
[32]P. Burgholzer, H. Roitner, J. Bauer-Marschallinger, and G. Paltauf, "Image reconstruction in photoacoustic tomography using integrating detectors accounting for frequency dependent attenuation," Proc. SPIE **7564**, 756400 (2010).
[33]A. D. Pierce, *Acoustics: An Introduction to its Physical Principles and Applications* (Acoustical Society of America, New York, 1989), pp. 316–318.
[34]T. L. Szabo, *Diagnostic Ultrasound Imaging* (Elsevier, Burlington, VT, 2004), p. 535.
[35]K. Firouzi, B. T. Cox, B. E. Treeby, and N. Saffari, "A first-order k-space model for elastic wave propagation in heterogeneous media," J. Acoust. Soc. Am. **132**, 1271–1283 (2012).
[36]B. Compani-Tabrizi, "*K*-space scattering formulation of the absorptive full fluid elastic scalar wave equation in the time domain," J. Acoust. Soc. Am. **79**, 901–905 (1986).
[37]M. Tabei, T. D. Mast, and R. C. Waag, "A k-space method for coupled first-order acoustic propagation equations," J. Acoust. Soc. Am. **111**, 53–63 (2002).
[38]T. D. Mast, L. P. Souriau, D.-L. D. Liu, M. Tabei, A. I. Nachman, and R. C. Waag, "A k-space method for large-scale models of wave propagation in tissue," IEEE Trans. Ultrason. Ferroelectr. Freq. Control **48**, 341–354 (2001).
[39]E. H. Saenger, N. Gold, and S. A. Shapiro, "Modeling the propagation of elastic waves using a modified finite-difference grid," Wave Motion **31**, 77–92 (2000).
[40]P. J. White, G. T. Clement, and K. Hynynen, "Longitudinal and shear mode ultrasound propagation in human skull bone," Ultrasound Med. Biol. **32**, 1085–1096 (2006).
[41]W. Legon, T. F. Sato, A. Opitz, J. Mueller, A. Barbour, A. Williams, and W. J. Tyler, "Transcranial focused ultrasound modulates the activity of

primary somatosensory cortex in humans," Nat. Neurosci. **17**, 322–329 (2014).
[42]R. L. King, J. R. Brown, W. T. Newsome, and K. B. Pauly, "Effective parameters for ultrasound-induced in vivo neurostimulation," Ultrasound Med. Biol. **39**, 312–331 (2013).
[43]J. Jaros, B. E. Treeby, and A. P. Rendell, "Use of multiple GPUs on shared memory multiprocessors for ultrasound propagation simulations," in *10th Australasian Symposium on Parallel and Distributed Computing*, edited by J. Chen and R. Ranjan (ACS, 2012), Vol. 127, pp. 43–52.